Synthesis of model sodium sulfide films

Rebecca D. McAuliffe, Victoria Petrova, Matthew J. McDermott, Jameson Landon Tyler, Ethan C. Self, Kristin A. Persson, Ping Liu, and Gabriel M. Veith

View Online   Export Citation   CrossMark

Synthesis of model sodium sulfide films

Rebecca D. McAuliffe,[1,a)] Victoria Petrova,[2] Matthew J. McDermott,[3,4] Jameson Landon Tyler,[1] Ethan C. Self,[1] Kristin A. Persson,[4,5] Ping Liu,[2] and Gabriel M. Veith[1]

AFFILIATIONS

[1]Chemical Sciences Division, Oak Ridge National Laboratory, Oak Ridge, Tennessee 37831
[2]Department of Nanoengineering, University of California-San Diego, La Jolla, California 92093
[3]Materials Sciences Division, Lawrence Berkeley National Laboratory, 1 Cyclotron Road, Berkeley, California 94720
[4]Department of Materials Science and Engineering, University of California, Berkeley, California 94720
[5]Molecular Foundry, Lawrence Berkeley National Laboratory, 1 Cyclotron Road, Berkeley, California 94720

Note: This paper is a part of the Special Topic Collection: Celebrating the Early Career Professionals Contributing to the Advancement of Thin Films, Surfaces, Interfaces, and Plasmas.
a)Electronic mail: mcaulifferd@ornl.gov

ABSTRACT

We report the direct deposition of model sodium sulfide films by RF magnetron sputtering from Na_2S and Na_2S_2 deposition targets. Analytical characterization and electrochemical cycling indicate that the deposited films are amorphous with stoichiometries that correspond to Na_2S_3 and Na_2S_2 formed from the Na_2S and Na_2S_2 targets, respectively. We propose that the loss of Na in the case of the Na_2S target is due to preferential sputtering of Na resulting from the higher energy required to break the Na–S bonds in Na_2S. The development of thin film sodium sulfides opens a new route to understanding their fundamental properties, such as Na^+ transport, conductivity, and reactivity.

Published under an exclusive license by the AVS. https://doi.org/10.1116/6.0001069

I. INTRODUCTION

Sodium sulfides play a significant role in a range of applications including serving as precursors in organic syntheses to synthesize thioamides[1,2] and for low-temperature synthesis of binary sulfides via solid-state metathesis reactions,[3] as well as in the precipitation of metals in wastewater treatment and dyes in textile manufacturing. Sodium sulfides, such as Na_2S and Na_2S_2, are also of interest as conversion cathodes in Na-based batteries due to their high theoretical energy density and low cost.[4–12] Despite the importance of these materials, research performed on the synthesis of sodium sulfides has been primarily focused on the synthesis of bulk powders. The synthesis routes investigated include direct elemental combination,[3] carbon reduction of Na_2SO_4,[13] microwave-assisted synthesis,[14] solution-based synthesis,[15] and drying of hydrated sodium sulfides.[16]

Thin film samples are important to synthesize as they provide a route to study (i) fundamental materials properties, such as diffusion constants, (ii) reaction mechanisms for solid-state reactions, and (iii) model battery electrode architectures. Thin film samples are key to studying electrodes as they do not contain conductive additives and polymer binders, which can complicate the characterization of the active material. Thin film transition-metal sulfides have been synthesized by a range of methods including chemical bath deposition,[17,18] thermal coevaporation,[19–21] sulfur vapor transport,[22] and RF magnetron sputtering,[23,24] but fewer investigations have been performed on alkali-metal sulfide thin films. Li_2S films have been synthesized by atomic layer deposition,[25] thermal evaporation,[26] and RF magnetron sputtering.[26,27] Na_2S films were synthesized by spray coating,[28] but no study has investigated the direct deposition of Na_2S and Na_2S_2 by RF magnetron sputtering.

Here, we report a method for the direct deposition of well-defined films of sodium sulfides by RF magnetron sputtering. The films have been characterized by x-ray diffraction (XRD), Raman spectroscopy, scanning electron microscopy (SEM), and cyclic voltammetry, which reveal that the starting target composition and structure dictated the stoichiometry of the final film.

II. EXPERIMENT

Na_2S powder was prepared by dehydrating $Na_2S \cdot 9H_2O$ (Alfa Aesar, 98.0%) under vacuum for 30 min at room temperature

followed by vacuum heating at 160 °C for 1 h. Na_2S_2 powder was synthesized from dehydrated Na_2S and elemental sulfur (Alfa Aesar, 99.5%). Stoichiometric amounts of Na_2S and S were ground and mixed using an agate mortar and pestle and heated in an Al_2O_3 crucible to 230 °C for 12 h. To fabricate the sputtering targets, the powders were ground using a mortar and pestle and pressed using a 2″-diameter die. The Na_2S and Na_2S_2 pellets were sintered and bound to copper backing plates. Due to the hygroscopic nature of sodium sulfides, all powder synthesis and target processing steps were performed inside an Ar-filled glovebox. All sample heating was performed in a box furnace that was placed inside an Ar-filled glovebox, and all heating rates were 5 °C/min, unless otherwise noted.

Films were deposited by RF magnetron sputtering using a deposition chamber that is integrated into an Ar-filled glovebox, as described in previous studies.[27,29] Na_2S films were deposited at a power of 70 W with an Ar pressure of 20 mTorr flowing at 20 SCCM. Na_2S_2 films were deposited at a power of 40 W with an Ar pressure of 11 mTorr flowing at 20 SCCM. The targets were presputtered for at least 2 h prior to deposition to remove any surface contamination. The plasma changed color from pink [Fig. 1(a)] to orange [Fig. 1(b)] when the target was ready to sputter.

XRD was performed using a Scintag XDS 2000 diffractometer with Cu-Kα radiation. Samples were prepared for XRD by placing the sample on a glass slide and covering the sample with Kapton tape to protect the sample from air and moisture. Rietveld refinements were performed using TOPAS version 6. Structures were visualized using VESTA.[30]

Raman spectra were acquired with an Alpha 300 confocal Raman microscope (WITec) using a solid-state 532 nm excitation laser. Laser power was maintained at 125 μW to mitigate thermal decomposition from laser-induced heating. Both samples were sealed in an electrochemical cell with a glass window prior to Raman measurement in an Ar-filled glovebox. Spectra were taken from five points on the sample to confirm sample uniformity. Background subtractions were performed using the WITEC PROJECT PLUS software.

Scanning electron micrographs and energy dispersive x-ray spectroscopy (EDX) spectra were acquired using a Zeiss Sigma

500 microscope with IRIDIUM ULTRA software. Samples were mounted on a sample holder using double-sided carbon tape and sealed in an aluminum lined bag within an Ar glovebox to be transported to the microscope with minimal exposure to ambient air. SEM images were taken at a 3.0 keV, while the EDX spectra used a 15 keV voltage.

Inductively coupled plasma optical emission spectroscopy (ICP-OES) measurements were carried out on a Thermo Scientific iCAP 7400 ICP-OES Duo. For analysis, the sulfide films were grown on polished silicon. Due to concern regarding the volatility of H_2S, these films were heated to 400 °C in dry oxygen to form a sulfate, which was then dissolved in aqua regia overnight and diluted with pure water (18 MΩ). TraceCert ICP standards were obtained from Sigma-Aldrich for instrument calibration.

Thin film electrodes were characterized using 2032-type coin cells and assembled in an Ar-filled glovebox. Sodium metal (Aldrich Dry Sticks) was cut and adhered to a stainless-steel spacer and served as the counter/reference electrode. Three 18 mm disks of the Dreamweaver Gold separator were placed on top of the sodium metal and then 50 μl electrolyte was added to the separator. The electrolyte used was 1.5 M $NaClO_4$/0.3 M $NaNO_3$ in tetraethylene glycol dimethyl ether.[9–11,14] A section of the film was then placed on top of the separator to serve as the working electrode. The coin cell was sealed using a hydraulic press. Cyclic voltammograms (CVs) were measured using a BioLogic system. CVs were measured between 1.2 and 3.0 V versus Na/Na+ with a potential sweep rate of 0.1 mV s^{-1} for 20 cycles.

The relative stabilities of Na_2S and Na_2S_2 are referenced from density functional theory (DFT) calculations using the r2SCAN metaGGA functional, with input settings given by the *MPScanRelaxSet* parameters in PYMATGEN.[31]

III. RESULTS AND DISCUSSION

Sodium sulfide precursors were synthesized using solid-state methods and characterized using XRD, shown in Fig. 2. For Na_2S, the resulting light-yellow powder contains Na_2S (Fm-3m) as the primary phase with Na_2SO_3 (P-3) and Na_2S_2 (P63/mmc) present at 4.7 and 2.2 wt. %, respectively, according to Rietveld refinements shown in Fig. 2(a). For Na_2S_2, the resulting dark-yellow powder contains β-Na_2S_2 (P63/mmc) as the primary phase with unreacted Na_2S and Na_2S_4 (I-42d) present at 4.8 and 13.2 wt. %, respectively, according to Rietveld refinements shown in Fig. 2(b). To model the scattering from the Kapton tape that covered the moisture-sensitive powders, four peaks at 14.5°, 18.1°, 21.7°, and 26.0° were added to the refinements. While these synthesis methods did not yield phase pure Na_2S or Na_2S_2 powders, they are an efficient way to make the quantity of powder (∼25 g) needed to fabricate the sintered targets with the right stoichiometry. Large batches of $Na_2S·9H_2O$ can be heated under vacuum, while reactions with Na metal and S powder would have to be performed in sealed ampoules in small (∼1–2 g) quantities due to safety concerns. Since the targets are atomized during the sputtering process, it is more important to have the correct Na:S ratios in the plasma than creating a phase pure target.

Films were deposited on an Al foil and characterized using x-ray diffraction. Na_2S and Na_2S_2 films were deposited for 2 and
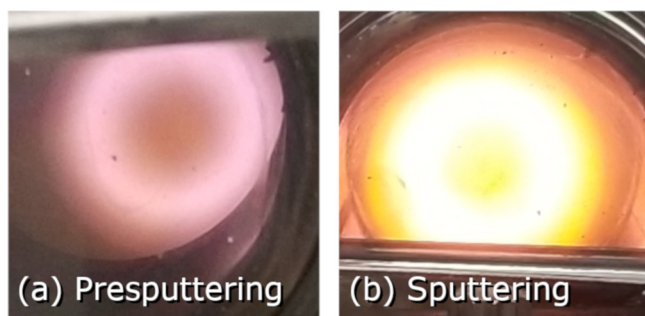

FIG. 1. Images of Na_2S_2 plasmas. Over the course of the presputtering process, the plasma changes from (a) a pale pink color during presputtering to (b) a bright orange as the surface layers are removed from the target.
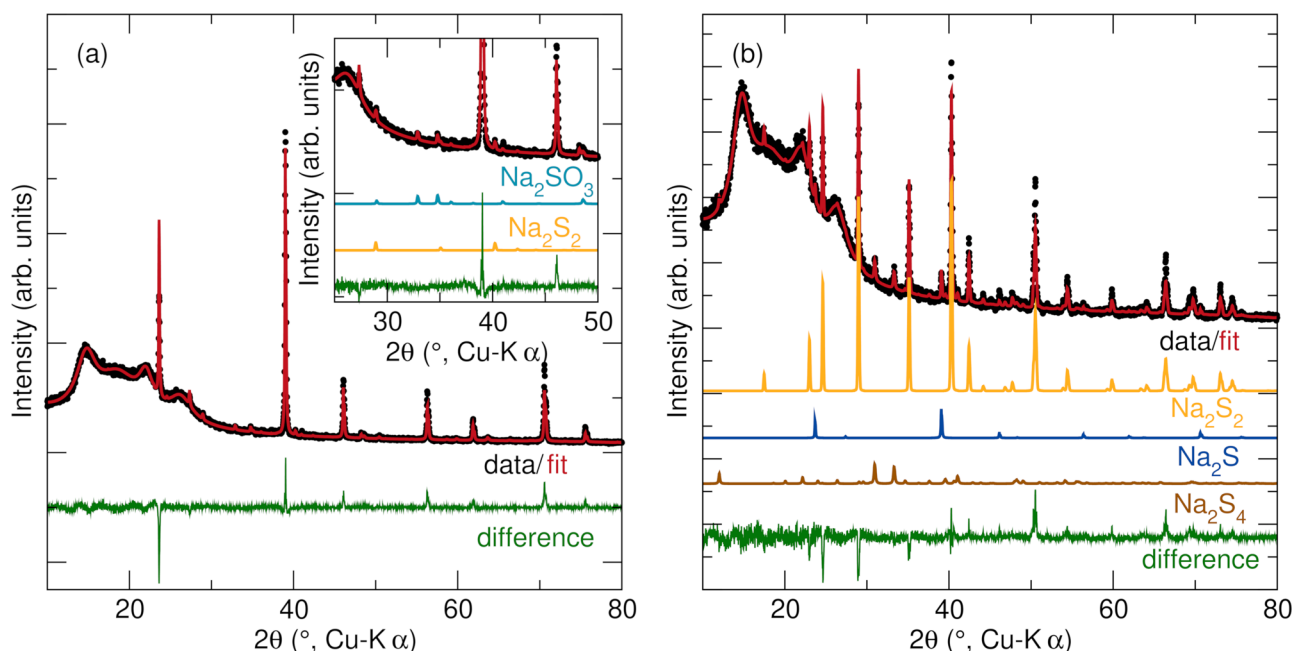
FIG. 2. Rietveld refinements of (a) Na_2S and (b) Na_2S_2 powder XRD patterns. Na_2S powder has Na_2S as the primary phase and Na_2SO_3 (4.7 wt. %) and Na_2S_2 (2.2 wt. %) as secondary phases. Na_2S_2 powder has β-Na_2S_2 as the primary phase and Na_2S (4.8 wt. %) and Na_2S_4 (13.2 wt. %) as secondary phases. Kapton background at low 2θ was modeled with four peaks. These materials were used as targets for the sputtered films.

12 h, respectively, and both films were pale yellow in color. XRD patterns of the as-deposited films showed only peaks from the Al foil substrate and from the Kapton tape used to cover the air-sensitive films indicating that the films are amorphous. Initial annealing studies showed some indication of increased crystallinity after 1 h at 200 °C; however, the annealed films had poor adhesion to the substrate, so all studies were performed on the amorphous films.

To further probe the structure of the films, Raman spectroscopy measurements were performed, shown in Figs. 3(a) and 3(b). Raman spectroscopy was also performed on the starting powders for reference, shown in Figs. 3(c) and 3(d). Two distinct regions were observed in the Na_2S powder, so representative spectra for each region are shown in Fig. 3(c). Raman spectroscopy was also performed on the Al foil to confirm that it was not Raman active. The Al foil had no observable peaks over the measured range. The spectra from the films sputtered using the Na_2S target, shown in Fig. 3(a), and have peaks at 241, 390, 478, and 947 cm^{-1}. The peaks for this film do not correspond to peaks associated with Na_2S (187, 324, and 420 cm^{-1}) but instead are similar to those for Na_2S_4 (239 and 471 cm^{-1}).[32,33] The spectra of starting Na_2S powder, shown in Fig. 3(c), has peaks at 138, 190, 455, 892, and 934 cm^{-1}. The peaks at 138 and 455 cm^{-1} are similar to the peaks associated with Na_2S_2 (133 and 450 cm^{-1}), and the peak at 190 cm^{-1} is similar to the most intense peak in previously reported Na_2S spectra, which was observed at 187 cm^{-1}.[32] The spectra from the Na_2S film is significantly different from the original starting

powder indicating a structural difference between the two materials.

The films sputtered using the Na_2S_2 target, shown in Fig. 3(b), show well-defined peaks at 145, 215, 415, 453, 591, 717, 1216, and 1275 cm^{-1}. The main peak at $\sim$450 cm^{-1} corresponds to the S–S stretching band in Na_2S_2.[32] The spectra of starting Na_2S_2 powder, shown in Fig. 3(d), has peaks at 138, 214, 245, 455, 484, and 893 cm^{-1}. The Na_2S_2 powder also has peaks similar to the peaks associated with Na_2S_2 (133 and 450 cm^{-1}) and also has a peaks at 245 and 484 cm^{-1}, which is similar to the peaks for Na_2S_4 (239 and 471 cm^{-1}).[33] The spectra from the Na_2S_2 film is similar to the original starting powder indicating a structural similarity between the two materials. These films and powders do not show any presence of hydrated phases as there are no OH bands present at either 1633 or 2800–3800 cm^{-1}.[34] There is also no evidence of S_8 since there are no S–S bending bands present at 153 or 220 cm^{-1}.[35] The peaks present in the films are broad with peaks overlapping. These spectra are similar to amorphous sulfides rather than highly crystalline compounds, which exhibit sharp, distinct peaks.[32] The Raman spectra show once again that the films are poorly crystalline with a combination of several phases present in the as-deposited samples.

Scanning electron micrographs show the film morphology, and SEM-EDX provides information about the composition of the deposited films. Micrographs show that the deposition of both Na_2S and Na_2S_2 targets yield continuous coatings covering the substrate, shown in Fig. 4. The analysis of the EDX spectra of the film
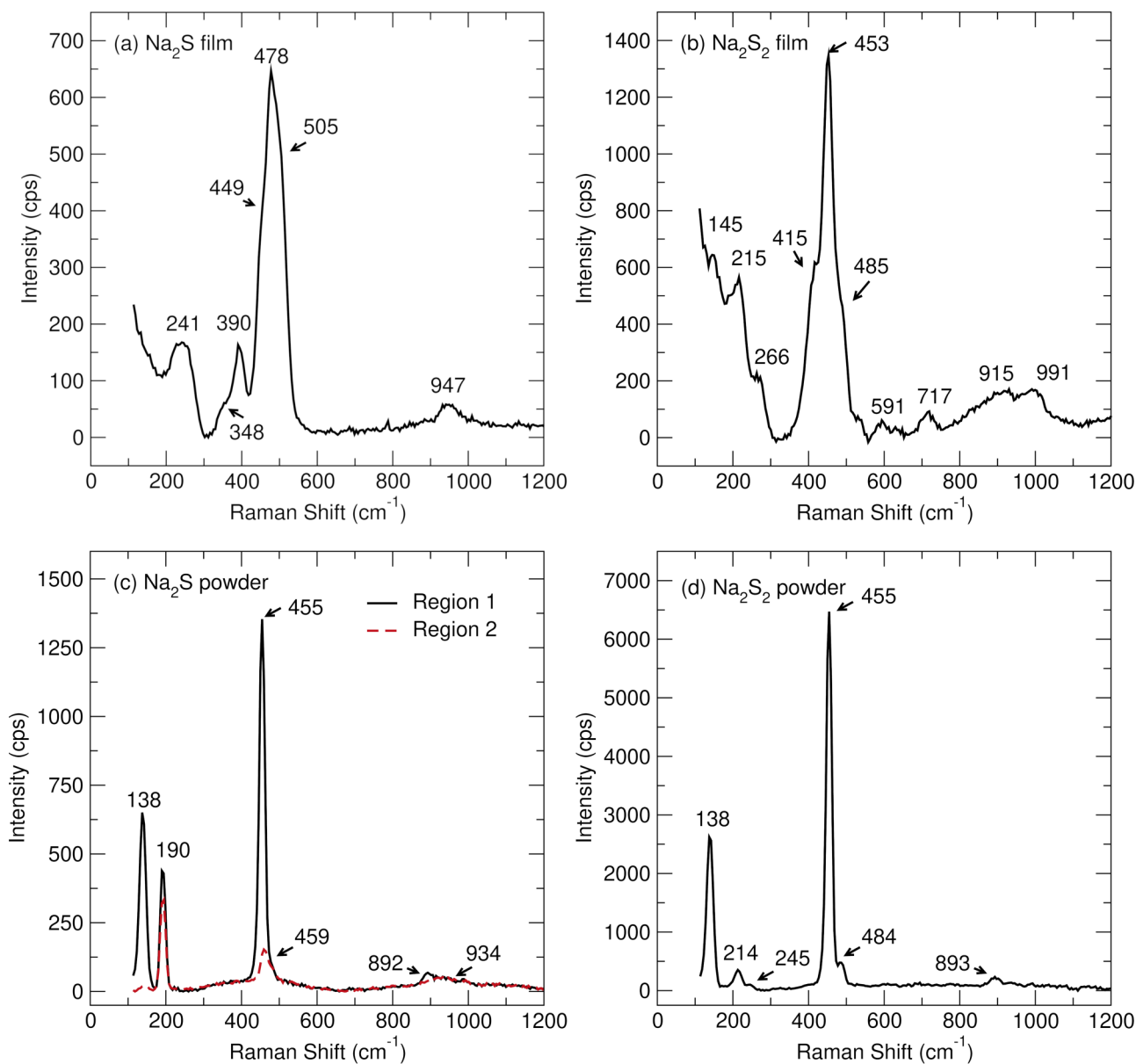
FIG. 3. Raman spectra from the films deposited using the (a) Na_2S target and the (b) Na_2S_2 target and the starting (c) Na_2S and (d) Na_2S_2 powders. Two distinct regions were observed while measuring the Na_2S powder and representative spectra are shown from each region. Intensity is shown in counts per second.

sputtered by the Na_2S target yielded a Na:S atomic ratio of 43:57. The ICP data produced a similar ratio of 43:57. This result shows that the films are Na-deficient when compared to Na_2S.

EDX of the film sputtered by the Na_2S_2 target yielded a Na:S atomic ratio of 54:46. ICP data collected on these samples produced similar atomic ratios of 56:44.This result shows that the films are slightly S-deficient when compared to the ideal Na_2S_2 composition.

CVs were used to characterize the electrochemical properties of the Na_2S_x films, as shown in Fig. 5. The films sputtered from the Na_2S target have an open circuit voltage (V_{OC}) of 1.96 V versus Na/Na^+. This value is higher than expected for an Na_2S film and corresponds to a more Na-deficient phase, supporting the results from the EDX measurements. Oxidation peaks appear for this film at ~2.0 and ~2.6 V corresponding to the removal of Na^+ ions from the electrode. The peak at 1.9 V corresponds to the formation of
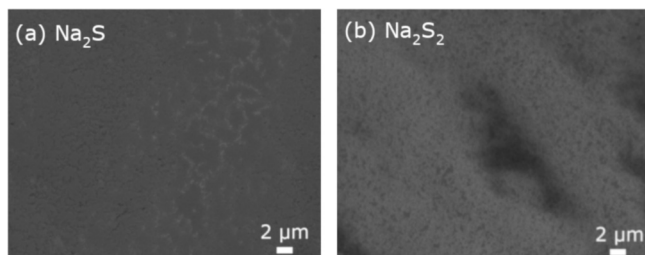
FIG. 4. Scanning electron micrographs of films deposited from (a) an Na_2S target and (b) an Na_2S_2 target on to Al foil.

Na_2S_6 and the peak at 2.6 V corresponds to the formation of higher order sodium polysulfides.[9] The reduction peaks for Na_2S are observed at ~1.9 and ~1.6 V. The peak at 2 V corresponds to the formation of Na_2S_5 and the peak at 1.6 V corresponds to the formation of Na_2S_3.[9] The films sputtered from the Na_2S_2 target have a V_{OC} of 1.48 V and oxidation peaks at ~2.0 and ~2.6 V. The reduction peaks are present at ~1.9 and ~1.7 V. The peak at 1.7 V corresponds to the formation of Na_2S_4.[9] The V_{OC} of the Na_2S_2 film is lower than that of the Na_2S film, which is consistent with differences in Na-content and the composition closer to a fully sodiated phase. The films sputtered with the Na_2S_2 target contain more Na than the films sputtered with the Na_2S target, which complements the findings of the SEM-EDX data. The peaks in the CVs decrease with each cycle as the film begins to dissolve into the electrolyte.

Depositing films from an Na_2S target yields an Na-deficient film while depositing films from an Na_2S_2 target does not. Composition discrepancies from the target to film are present in the deposition of many compounds including CaF_2,[36] Li_4SiO_4,[37] phosphate glasses,[38] and many metal alloys,[39,40] and several mechanisms have been proposed to explain for preferential sputtering of specific atoms. One mechanism is negative ion formation that leads to a negative accumulation rate, or etching, of the deposited material. Cuomo *et al.* provide a threshold to predict which compounds will suffer from negative ion etching based on the ionization potential and the electron affinities of the compounds.[39] While Na_2S falls within the predicted range, so does Na_2S_2. Using this method, both materials should lead to Na-deficient films, but this is not what is observed experimentally. Another possible mechanism is target decomposition leading to material redistribution. This process has been observed in Li_4SiO_4 where the target becomes discolored, and Li_2O forms in the center of the target where sputtering does not occur, resulting in an Li deficient film.[37] However, in this study, no target decomposition or redistribution within the target was observed. Another mechanism is related to the overall bond strength of different components in multicomponent systems. For example, in phosphate glasses, the sputtering rate of different atoms correlates to the dissociation energy per bond within the structure; phosphorous has strong covalent bonds within the structure and has the lowest sputtering yield of the five cations present in the system.[38] While there is not a range of bonds present within Na_2S, there is a significant difference between the formation enthalpies of Na_2S and Na_2S_2. The formation enthalpies of Na_2S and Na_2S_2, calculated by DFT (r2SCAN), are -1.269 and
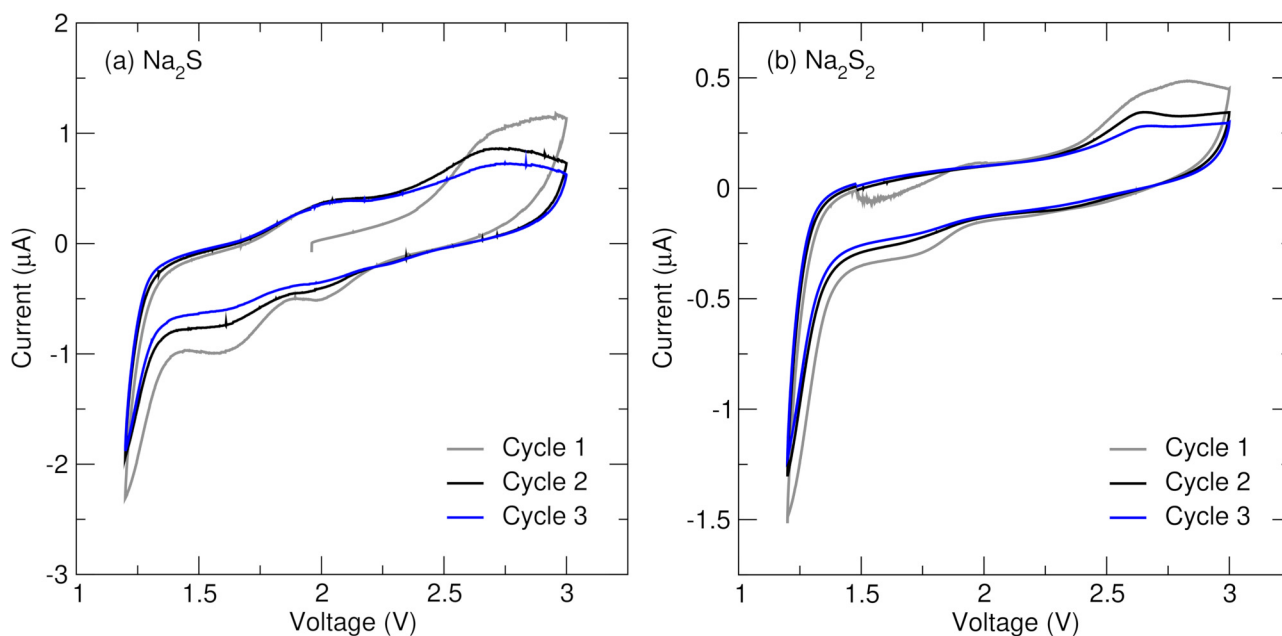

FIG. 5. First three cyclic voltammograms of films sputtered by targets composed of (a) Na_2S and (b) Na_2S_2 films cycled against Na metal between 1.2 and 3.0 V.

−1.004 eV/atom, respectively, indicating that Na_2S is a significantly more thermodynamically stable compound by about 0.265 eV/atom. This calculated value also agrees well with the experimentally measured difference of +0.246 eV/atom at 298 K.[41]

We hypothesize that the primary cause of the observed Na-deficiency in the deposited film is the increased preferential resputtering of Na due to the higher energies required for sputtering of the more stable Na_2S target. The increased resputtering is a direct consequence of the predicted increase in surface binding energies of Na and S in the Na_2S compound. Although the actual surface binding energies for species in an ionic compound are difficult to calculate and depend on several unknown parameters,[42] they have been suggested to correlate directly with the enthalpy of formation of the compound.[43] Thus, the extra energy needed to break the Na–S bonds and atomize Na_2S results in higher energies of the sputtered atoms and hence an increased possibility for resputtering, where atoms deposited on the substrate are ejected from the deposited film. Resputtering tends to affect lighter elements more significantly,[40] and the significantly lower atomization enthalpy of Na (107.3 kJ/mol) versus S (278.8 kJ/mol) further suggests that Na may be more susceptible to resputtering.[44] Since there is less energy needed to deposit the Na_2S_2 films, as highlighted in the differences in sputtering power (70 vs 40 W), the resputtering is less pronounced in films deposited using the Na_2S_2 target. This resputtering effect can be mitigated by changing the sputtering geometry in future studies.[36]

IV. SUMMARY AND CONCLUSIONS

This paper presents the first deposition of sodium sulfides by RF magnetron sputtering and continues to build on the work being done to deposit films of alkali sulfides for energy storage applications. Na_2S and Na_2S_2 deposition targets were fabricated and sputtered onto Al foil to create model sulfide films with two distinct compositions. X-ray diffraction patterns showed that the films deposited from the Na_2S and Na_2S_2 targets were amorphous. SEM micrographs show that the films are continuous across the substrate and are not porous. The SEM-EDX data revealed that the film deposited using the Na_2S target is Na-deficient with an overall stoichiometry close to Na_2S_3, while the film deposited using the Na_2S_2 target is S-deficient, but close to the ideal composition of Na_2S_2. We propose that the Na-deficiency present in Na_2S is due to increased resputtering of Na when depositing Na_2S as a result of the higher energies needed to atomize Na_2S compared to Na_2S_2 based on the compound's thermodynamic stability. This effect can be alleviated by further optimization of the deposition geometry. Cyclic voltammetry measurements of the films correspond well with previously published studies showing that the films can be used as cathodes for Na-based batteries. Future studies with these films are needed to optimize the films and prevent the dissolution of the films into the electrolyte. These thin films can be used in Na–S batteries as well as in thin film heterostructures and devices, providing new ways to study these critical compounds.

ACKNOWLEDGMENTS

DATA AVAILABILITY

The data that support the findings of this study are available from the corresponding author upon reasonable request.

REFERENCES

[1]Y. Sun, H. Jiang, W. Wu, W. Zeng, and J. Li, Org. Biomol. Chem. **12**, 700 (2014).
[2]J. Wei, Y. Li, and X. Jiang, Org. Lett. **18**, 340 (2016).
[3]A. J. Martinolich and J. R. Neilson, J. Am. Chem. Soc. **136**, 15654 (2014).
[4]Y. X. Wang, B. W. Zhang, W. H. Lai, Y. F. Xu, S. L. Chou, H. K. Liu, and S. X. Dou, Adv. Energy Mater. **7**, 1602829 (2017).
[5]A. Manthiram and X. Yu, Small **11**, 2108 (2015).
[6]S. Xin, Y. X. Yin, Y. G. Guo, and L. J. Wan, Adv. Mater. **26**, 1261 (2014).
[7]D. J. Lee, J. W. Park, I. Hasa, Y. K. Sun, B. Scrosati, and J. Hassoun, J. Mater. Chem. A **1**, 5256 (2013).
[8]X. Yu and A. Manthiram, Chem. Mater. **28**, 896 (2016).
[9]X. Yu and A. Manthiram, ChemElectroChem **1**, 1275 (2014).
[10]X. Yu and A. Manthiram, J. Phys. Chem. Lett. **5**, 1943 (2014).
[11]X. Yu and A. Manthiram, Chem. Eur. J. **21**, 4233 (2015).
[12]X. Yu and A. Manthiram, Adv. Energy Mater. **5**, 1500350 (2015).
[13]E. Feldbaumer, H. Loquenz, and A. Sandri, U.S. patent 4,198,385 (15 April 1980).
[14]H. El-Shinawi, E. J. Cussen, and S. A. Corr, Inorg. Chem. **57**, 7499 (2018).
[15]T. Takata, D. Saeki, Y. Makita, N. Yamada, and N. Kihara, Inorg. Chem. **42**, 3712 (2003).
[16]K. Maeda and Y. Aoyama, U.S. patent 5,173,088 (22 December 1992).
[17]S. Hariech, M. S. Aida, J. Bougdira, M. Belmahi, G. Medjahdi, D. Genève, N. Attaf, and H. Rinnert, J. Semicond. **39**, 034004 (2018).
[18]B. Abdallah, R. Hussein, N. Al-Kafri, and W. Zetoun, Iran. J. Sci. Technol. Trans. A: Sci. **43**, 1371 (2019).
[19]B. H. Kumar, S. Shaji, and M. C. S. Kumar, Thin Solid Films **697**, 137838 (2020).
[20]V. Robles, J. F. Trigo, C. Guillén, and J. Herrero, J. Alloys Compd. **642**, 40 (2015).
[21]K. Benyahia, A. Benhaya, and M. S. Aida, J. Semicond. **36**, 103001 (2015).
[22]H. Dahman, M. Khalifa, M. Brunel, and B. Rezig, Thin Solid Films **280**, 56 (1996).

[23] D. H. Hwang, J. H. Ahn, K. N. Hui, K. S. Hui, and Y. G. Son, Nanoscale Res. Lett. **7**, 26 (2012).

[24] D. Shin, S. Lee, D. R. Kim, J. H. Park, Y. Kim, W.-J. Choi, C. S. Son, Y. G. Son, and D. Hwang, Energies **13**, 688 (2020).

[25] X. Meng, D. J. Comstock, T. T. Fister, and J. W. Elam, ACS Nano **8**, 10963 (2014).

[26] S. Lorger, D. Fischer, R. Usiskin, and J. Maier, J. Vac. Sci. Technol. A **37**, 061515 (2019).

[27] M. J. Klein, G. M. Veith, and A. Manthiram, J. Am. Chem. Soc. **139**, 10669 (2017).

[28] D. B. Chrisey, R. E. Johnson, J. W. Boring, and J. A. Phipps, Icarus **75**, 233 (1988).

[29] R. D. McAuliffe, G. Yang, J. Nanda, and G. M. Veith, Thin Solid Films **689**, 138520 (2019).

[30] K. Momma and F. Izumi, J. Appl. Cryst. **44**, 1272 (2011).

[31] S. P. Ong et al., Comput. Mater. Sci. **68**, 314 (2013).

[32] G. J. Janz, J. R. Downey, E. Roduner, G. J. Wasilczyk, J. W. Coutts, and A. Eluard, Inorg. Chem. **15**, 1759 (1976).

[33] Q. Zhang, "The synthesis and characterization of sodium polysulfides for Na-S battery application," Master's thesis (Virginia Polytechnic Institute and State University, 2019).

[34] K. B. Mabrouk, T. H. Kauffmann, H. Aroui, and M. D. Fontana, J. Raman Spectrosc. **44**, 1603 (2013).

[35] C. Nims, B. Cron, M. Wetherington, J. Macalady, and J. Cosmidis, Sci. Rep. **9**, 7971 (2019).

[36] N. J. Dudney, J. Vac. Sci. Technol. A **16**, 615 (1998).

[37] N. J. Dudney, J. B. Bates, and J. D. Robertson, J. Vac. Sci. Technol. A **11**, 377 (1993).

[38] B. Stuart, M. Gimeno-Fabra, J. Segal, I. Ahmed, and D. M. Grant, Thin Solid Films **589**, 534 (2015).

[39] J. J. Cuomo, R. J. Gambino, J. M. E. Harper, J. D. Kuptsis, and J. C. Webber, J. Vac. Sci. Technol. **15**, 281 (1978).

[40] S. Berg and I. V. Katardjiev, J. Vac. Sci. Technol. A **17**, 1916 (1999).

[41] I. Barin, in Thermochemical Data of Pure Substances (VCH, New York, 1995), Vol. 1.

[42] R. Kelly, Nucl. Instrum. Methods Phys. Res. Sect. B **18**, 388 (1987).

[43] E. Dullni, Nucl. Instrum. Methods Phys. Res. Sect. B **2**, 610 (1984).

[44] A. M. James and M. P. Lord, Macmillan's Chemical and Physical Data (Macmillan, London, 1992).

Victoria Petrova is pursuing a Ph.D. in the materials science and engineering department at the University of California, San Diego. Her research in the Liu group is focused on using conversion reactions to synthesize new nanomaterials, which are then characterized using electron microscopy and x-ray diffraction. These nanomaterials have a high surface area to volume ratio and have applications in catalysis and energy storage devices. She is also working on conversion batteries in which a better understanding of the mechanisms behind conversion reactions is needed to enable their higher capacity and improve their cycling stabilities. She hopes to continue researching batteries and working in renewable energy after graduate school in industry.
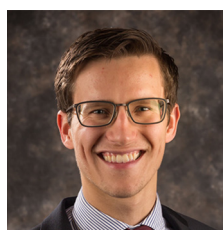
Matthew J. McDermott is a Ph.D. candidate in Materials Science and Engineering at the University of California, Berkeley. He works in Professor Kristin Persson's research group at the Lawrence Berkeley National Laboratory, which studies the chemistry of materials using high-throughput atomistic computational methods. His research focuses on the development of computational models for planning and understanding solid-state materials synthesis.

Jameson Landon Tyler received his B.S. in Chemical Engineering from the Tennessee Technological University (2016). After graduating, he interned at the Oak Ridge National Laboratory (ORNL) working on lithium ion batteries. He is now continuing his work in a joint program between ORNL and the University of Tennessee Knoxville to earn his Ph.D. in Energy Science and Engineering. His current research focuses on electrolyte optimization for various electrochemical storage devices.

Rebecca D. McAuliffe is a materials chemist whose research focuses on understanding reaction mechanisms that guide the syntheses of energy materials using x-ray and neutron diffraction. She focuses on developing tools to observe and model ion diffusion through interfaces using thin film heterostructures and powders. She received her B.S. in physics from Marquette University (2013), and Ph.D. from the University of Illinois at Urbana-Champaign (2018). Upon finishing her Ph.D. on materials discovery, she joined Oak Ridge National Laboratory as a postdoctoral fellow in the Energy Storage and Conversion group.

Ethan C. Self received his B.S. in chemical engineering from the University of Illinois Urbana-Champaign (2011) and Ph.D. in chemical engineering from the Vanderbilt University (2016). During graduate school, he completed a six-month internship at Merck KGaA (Darmstadt, Germany) developing electrospun catalyst layers for hydrogen-air fuel cells. He joined the Oak Ridge National Laboratory in 2017 and is currently an R&D Associate in the Energy Storage and Conversion Group. His research focuses on new materials and systems for electrochemical energy storage including (i) high energy density Li-ion batteries, (ii) all-solid-state batteries, and (iii) redox flow batteries.